Molecular Dynamics of the Ultrafast Excited-State Proton Transfer of the Super-Photoacid NM7HQ$^+$ to the Aprotic Solvent DMSO

Niklas Sülzner,[*,†,‡] Rafael Souza Mattos,[†] and Mario Barbatti[*,†,¶]

†*Aix Marseille University, CNRS, ICR, Marseille 13397, France.*

‡*Ruhr-Universität Bochum, Universitätsstr. 150, 44801 Bochum, Germany.*

¶*Institut Universitaire de France, Paris 75231, France.*

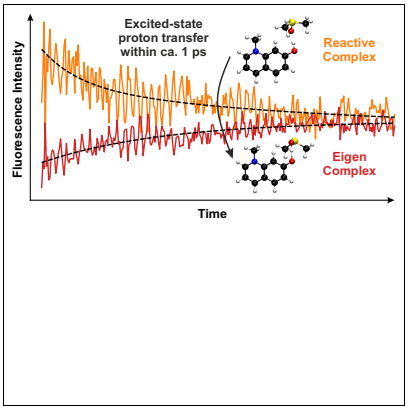
E-mail: niklas.suelzner@rub.de; mario.barbatti@univ-amu.fr

https://doi.org/10.26434/chemrxiv-2025-90jkg **ORCID:** https://orcid.org/0000-0002-8734-5807 Content not peer-reviewed by ChemRxiv. **License:** CC BY 4.0

Abstract

Photoacids exhibit an increase in acidity upon electronic excitation, providing powerful tools for studying excited-state proton transfer (ESPT) reactions. While these photoacids have been used extensively in experiments, theoretical studies, particularly on the dynamics, are largely lacking. Here, we report on the ultrafast ESPT of the super-photoacid *N*-methyl-7-hydroxyquinolium ($NM7HQ^+$) to the aprotic solvent DMSO, studied using excited-state ab initio molecular dynamics (AIMD). We combine TDDFT with the implicit solvent model PCM to simulate 400 trajectories for 3 ps, starting in the S_1 state. Our simulations reveal a short-lived equilibrium between the initially excited photoacid-DMSO complex (CPX) and the so-called Eigen complex (EC), the ESPT product, established within 1 ps. Subsequently, the EC undergoes a slow separation via a rotational motion on the ps timescale, further driving the ESPT. These results imply that the ESPT within the CPX may be significantly faster (< 1 ps) than previously expected (2–3 ps).

TOC Graphic



Keywords

Photoacids, ESPT, AIMD, Excited-State Dynamics, Nonadiabatic Dynamics, Surface Hopping, TDDFT, Fluorescence, Spectroscopy

https://doi.org/10.26434/chemrxiv-2025-90jkg **ORCID:** https://orcid.org/0000-0002-8734-5807 Content not peer-reviewed by ChemRxiv. **License:** CC BY 4.0

Main Text

Proton transfer in both the electronic ground and electronically excited states is of fundamental importance in chemistry and related fields.[1–3] Examples are countless and omnipresent, ranging from acid–base catalysis[4] and proton membranes in fuel cells,[5] to diverse biochemical mechanisms,[6,7] such as proton transfer in electronically excited states of various biological chromophores.[8–10] In this context, photoacids, i.e., compounds that undergo an acidity increase upon electronic excitation, play a central role. Prototypical examples of photoacids are the neutral hydroxy (OH) and cationic ammonium (NH_3^+) aromatic compounds.[11,12] Apart from various applications including photocatalysis,[13] bioimaging,[14] and single-molecule microscopy[15] (e.g., see Ref. 11 for a recent review), these photoacids have been established as powerful tools for probing excited-state proton transfer (ESPT) reactions by offering a precise time control, e.g., when using pulsed lasers.

The ESPT of photoacids has been extensively studied with respect to different environments, spectroscopic techniques, and theory (as recently reviewed in Ref. 12). For example, ESPT in aqueous solution has been demonstrated to follow an Eigen-Weller model:[16–18]

$$\begin{aligned} \mathrm{AH}^* + \mathrm{B} \overset{(1)}{\rightleftharpoons} \underbrace{[\mathrm{AH}^* \cdot \mathrm{B}]}_{\mathrm{CPX}} \overset{(2)}{\rightleftharpoons} \underbrace{[\mathrm{A}^{-*} \cdot \mathrm{HB}^+]}_{\mathrm{HBIP}} \\ \overset{(3)}{\rightleftharpoons} \underbrace{[\mathrm{A}^{-*} \cdots \mathrm{HB}^+]}_{\mathrm{SSIP}} \overset{(4)}{\rightleftharpoons} \underbrace{\mathrm{A}^{-*} + \mathrm{HB}^+}_{\mathrm{FIP}}. \end{aligned} \tag{1}$$

In its most general form, this model involves four steps and five photoacid species, accounting for: (1) The formation of a reactive encounter complex ($[\mathrm{AH}^* \cdot \mathrm{B}]$, CPX) *via* diffusion of the free excited photoacid (AH^*) and the proton-accepting base (B); (2) the fast proton transfer within the CPX under the formation of a (hydrogen-bonded) contact-ion pair ($[\mathrm{A}^- \cdot \mathrm{HB}^+]$, CIP/HBIP); (3) the step-wise diffusive separation of the HBIP into various solvent-separated ion pairs ($[\mathrm{A}^- \cdots \mathrm{HB}^+]$, SSIP); and (4) the final separation into the fully separated (or free) ion pair ($\mathrm{A}^{-*}/\mathrm{HB}^+$, FIP). Only step (2) is easily accessible in molecular dynamics (MD)

https://doi.org/10.26434/chemrxiv-2025-90jkg **ORCID:** https://orcid.org/0000-0002-8734-5807 Content not peer-reviewed by ChemRxiv. **License:** CC BY 4.0

simulations due to computational limitations regarding the other diffusive steps.

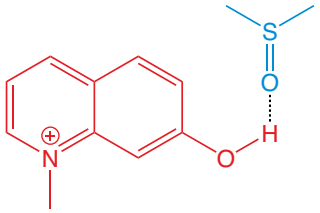


Figure 1: Molecular structures of the complex (CPX) between the super-photoacid $NM7HQ^+$ (in red) and the aprotic solvent DMSO (in blue).

The photoacid strength as quantified by pK_a^* (i.e., pK_a in the excited state; usually S_1) is decisive for the ESPT characteristics in different environments. While weak and moderately strong photoacids ($pK_a^* > 0$) are sufficient for ESPT in water due to effective proton stabilization *via* hydrogen bonding (HB), non-aqueous solutions, particularly aprotic solvents, require much stronger super-photoacids (with $pK_a^* < 0$).[12,19] One of these super-photoacids established for the study of non-aqueous ESPT is *N*-methyl-7-hydroxyquinolinium ($NM7HQ^+$; see Fig. 1), characterized by $pK_a = 5.9$ and $pK_a^* = -2.3$.[20] This photoacid was first introduced by Kim and Topp,[21] who revived the original idea of Bardez *et al.*[22] of blocking the photobasic nitrogen site in quinolines with a methyl (CH_3) group. Not only does this methylation switch off the competing photobasicity, it also enhances the photoacidity compared to the parent 7-hydroxyquinoline (7HQ; $pK_a = 8.7$, $pK_a^* = 0.4$).[23] Both 7HQ[24–32] and $NM7HQ^+$[20,33–43] have received extensive, ongoing attention by the group of Kwon, with a special focus on the role of hydrogen bonding and hydrogen-bonded solvent chains in the ESPT. The ESPT in hydrogen-bonded complexes of $NM7HQ^+$ with alcohols,[20,34,35] dimethyl sulfoxide (DMSO),[34,41,42] and *N*-methylbenzamide[40] in acetonitrile solution as well as in diols[36] has been investigated.

Owing to its positive charge in the non-dissociated form, $NM7HQ^+$ represents a special type of a photoacid (cf. note[44]). Since the corresponding base (A) of a positively charged photoacid (AH^+) is charge neutral, the proton transfer (step 2, Eq. (1)) within CPX does not yield an HBIP, but a so-called Eigen complex (EC) of the form $[A^* \cdot HB^+]$ instead.

https://doi.org/10.26434/chemrxiv-2025-90jkg **ORCID:** https://orcid.org/0000-0002-8734-5807 Content not peer-reviewed by ChemRxiv. **License:** CC BY 4.0

Therefore, the ESPT mechanism of such a super-photoacid in aprotic solvents is effectively terminated at step 3 in the ESPT mechanism (Eq. (1)). However, this termination step has only been recently successfully studied for the first time by Kwon and co-workers, at the example of $NM7HQ^+$ in DMSO–acetonitrile mixtures[41,42] First, they found a 1:1 hydrogen-bonded CPX between $NM7HQ^+$ and DMSO as a prerequisite for the ESPT to yield the EC as a transient intermediate. The general importance of such an EC as a short-lived, rarely observed ESPT intermediate has been recently discussed in Ref. 45. Second, they demonstrated the subsequent separation of the EC under the involvement of a second DMSO molecule into a Zundel-like cation $[(DMSO)_2 \cdot H^+]$. Focusing on the EC formation upon collisional ESPT (on the ns timescale), the authors omitted the contribution from ESPT after direct excitation of pre-existing CPX, as they monitored the slower dynamics and paid less attention to the ultrashort timescale. Resolving the ultrafast dynamics of the initial proton transfer (ca. 2–3 ps) is experimentally harder due to finite time resolutions (typically a few 100 fs), but falls into the regime feasible for molecular dynamics simulations.

Existing studies on the ESPT mechanism have predominantly focused on the PT step, partially due to the challenging conditions of protic solvents, especially water (e.g., short lifetimes of the intermediates), but also intentionally as part of a race among super-photoacids toward increasingly fast ESPT. Simkovitch *et al.* proposed a division of the existing set of photoacids into four regimes according to their pK_a^* and suggested a theoretical solvent-controlled limit for the ESPT rate of 10^{13} s^{-1} (100 fs).[46] While ESPT rates in protic solvents are (due to higher proton conductivities) significantly higher compared to aprotic ones, the latter provide simpler environments that lack extensive HB networks (due to their missing HB donation), overall enhancing the lifetime of the ESPT intermediates. Thus, using a super-photoacid in an aprotic solvent is an ideal environment for selectively probing the initial PT in the ESPT mechanism (step 2 in Eq. (1)).

In contrast to the wealth of experimental studies, theoretical studies on the ESPT—particularly regarding the dynamics and using simulation techniques—are still scarce, mostly

https://doi.org/10.26434/chemrxiv-2025-90jkg **ORCID:** https://orcid.org/0000-0002-8734-5807 Content not peer-reviewed by ChemRxiv. **License:** CC BY 4.0

focusing on the much faster intramolecular ESPT (ESIPT) reactions.[47–49] Importantly, studying the actual dynamics of the ESPT—as an excited-state reaction—requires *ab initio* molecular dynamics (AIMD) techniques for electronically excited states, which also allow for changes in the electronic state, i.e., nonadiabatic effects.[50] The most used technique for nonadiabatic dynamics is the surface-hopping approach,[51] which has been applied to study ESIPT.[52] To the best of our knowledge, no nonadiabatic studies have been reported on intermolecular ESPT (only adiabatic ones[53–64]), nor on ESPT in non-aqueous solutions

In this work, we study the ultrafast intermolecular ESPT of the super-photoacid $NM7HQ^+$ to the aprotic solvent DMSO (Fig. 1) using *ab initio* molecular dynamics (AIMD) in the S_1 excited state. We apply time-dependent density functional theory (TDDFT; ωB97X-D) for the electronic structure and the polarizable continuum model (PCM) for implicit solvation. The system is given the possibility to relax into the S_0 ground state *via* surface hopping, but no hops are observed, effectively showcasing the adiabatic dynamics in S_1. This particular combination of photoacid and base has been chosen because it is the smallest example of ESPT in a non-aqueous solution for which direct experimental reference data are available. Thereby, we provide additional information on the mechanistic details of the ESPT in a non-aqueous solution, representing one of the few AIMD studies on intermolecular ESPT.

Preliminary Static Calculations At the S_0 equilibrium structure of the $NM7HQ^+$–DMSO complex (referred to as **CPX**), the strongest UV/Vis absorption at 4.1 eV can be assigned to a transition into the bright S_1 state with $\pi \rightarrow \pi^*$ character (see Fig. 2). Due to usage of the equilibrium conditions for PCM (i.e., using the refractive index instead of the dielectric constant) when treating excited states, the corresponding emission energy at the same S_0 structure (with the solvent equilibrated to S_0) is 4.0 eV with the solvent equilibrated to S_1. From this Franck-Condon (**FC**) point, the structure relaxes into the S_1 equilibrium with an emission energy of 3.6 eV. A significant contribution to this Stokes shift is the contraction (13 pm) of the HB to DMSO, in parallel to a slight elongation (5 pm) of

https://doi.org/10.26434/chemrxiv-2025-90jkg **ORCID:** https://orcid.org/0000-0002-8734-5807 Content not peer-reviewed by ChemRxiv. **License:** CC BY 4.0

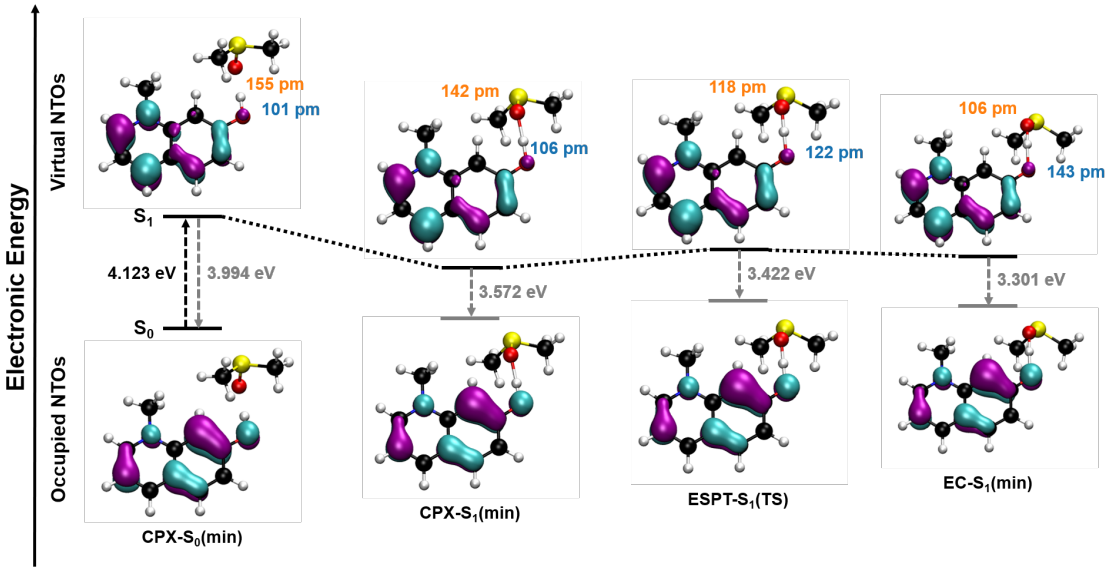


Figure 2: Reaction path for the ESPT from $NM7HQ^+$ to DMSO. Optimized structures for the S_0 and S_1 minima of **CPX**, the ESPT transition state (**TS**), and the S_1 minimum of **EC** (i.e., after ESPT) are shown. The energies for the initial $S_0 \rightarrow S_1$ absorption (in black) and $S_1 \rightarrow S_0$ emission (in gray) are given. O–H distances for the donating photoacid (in blue) and accepting DMSO (in orange) are included. The occupied and virtual parts of the dominant NTO pairs are shown in the bottom and top structures, respectively.

the O–H bond in $NM7HQ^+$, constituting an overall strengthening of the HB. The ESPT in the **CPX** proceeds *via* a transition state (**TS**) with an (electronic) activation energy of ca. 3 kJ mol^{-1}, in which the proton is almost symmetrically shared between the donor (122 pm) and acceptor (118 pm) oxygen atoms at the photoacid and $NM7HQ^+$, respectively. At an overall energetic cost in the same order of magnitude (ca. 2 kJ mol^{-1}), the product of the ESPT, i.e., the so-called Eigen complex (**EC**) is formed, in which the proton resides at the acceptor site of the DMSO (106 pm) with a significantly larger distance to the donor O of the photoacid (143 pm). It should be noted that the emission energies of the **TS** (3.4 eV) and the **EC** (3.3 eV) are very similar and that the character of the S_1 remains the same in **CPX**, **TS**, and **EC** (cf. Table S1; Supporting Information, SI). Only after a complete separation (i.e., at an infinite distance), the emission of the free base species reaches a value of 3.1 eV, with an O–H distance of 96 pm in the protonated DMSO, additionally ca. 30 kJ mol^{-1} lower in energy compared to the **EC**.

https://doi.org/10.26434/chemrxiv-2025-90jkg **ORCID:** https://orcid.org/0000-0002-8734-5807 Content not peer-reviewed by ChemRxiv. **License:** CC BY 4.0

Table 1: Comparison of the calculated and experimental characteristic properties, i.e., absorption and emission energies [in eV (nm)] and emission lifetimes (in ns) of the different chemical species in DMSO.

	Absorption		Emission		Lifetime	
	Calc.[a]	Exptl.[b]	Calc.[a]	Exptl.[b]	Calc.[a]	Exptl.[b]
ROH$^+$	4.350	3.54	3.815	2.88	4.3	9.12[c]
	(285)	(350)	(325)	(430)	—	$\sim$ 6.8–7.5[d]
RO	3.631	2.75	3.086	2.34	7.3	6.5
	(341)	(450)	(402)	(530)	—	—
CPX	4.123	3.30	3.572	2.83	5.4	n.a.
	(301)	(375)	(347)	(438)	—	—
EC	n.a.	n.a.	3.301	2.58	5.1	n.a.
	(n.a.)	(n.a.)	(376)	(480)	—	—

[a] PCM-RI-TDA-TDDFT(ωB97X-D)/def2-SVP
[b] Taken from Refs. 41,42
[c] In acetonitrile (MeCN)
[d] Value in DMSO estimated from that in MeCN using $\tau \propto n^{-p}$ $(p = 2, 3)$[65] with the refractive indices n (DMSO: 1.479; MeCN:1.344).[66]

While the level of theory applied here systematically overestimates the absolute absorption and emission energies by ca. 0.7–0.8 eV compared to the experimental band maxima (see Table 1), the relative energy differences (e.g., Stokes shifts) are reproduced reasonably well with deviations of only 0.1–0.2 eV. In particular, the experimental shift between **CPX** (2.83 eV) and **EC** (2.58 eV) emission of 0.25 eV is nicely reproduced by the calculations (ca. 0.27 eV). The energy difference between the excited acid (ROH^{+*}) and conjugated base (RO^*) suggests an acidity jump $\Delta pK_a^* = pK_a^* - pK_a$ upon excitation of -8.2 based on the Förster cycle (see SI),[67] in perfect agreement with the experimental value.[20] Moreover, the fluorescence lifetimes calculated based on the spontaneous emission rate (cf. Eq. (2)) are in fair agreement with the experimental ones. Second-order wavefunction-based methods like ADC(2) or CC2 combined with PCM get closer to the experimental band maxima, but as post-HF methods their combination with an implicit solvent model raises the known issue of selecting an appropriate coupling scheme for the self-consistent reaction field (SCRF) procedure to include solvent effects beyond the HF level (see Tab. S2 and its discussion in the SI),[68] in addition to their significantly higher computational costs. At all relevant

https://doi.org/10.26434/chemrxiv-2025-90jkg **ORCID:** https://orcid.org/0000-0002-8734-5807 Content not peer-reviewed by ChemRxiv. **License:** CC BY 4.0

configurations (i.e., **CPX**, **TS**, and **EC**) in S_1, S_1 is separated by at least 1 eV from S_2 and higher states, with S_2 being significantly less bright (cf. Table S3, SI). Besides, errors due to the small basis-set size or absence of diffuse functions were found to be not an issue (cf. Table S2, SI). Thus, this TDA-TDDFT level of theory is considered satisfactory for the AIMD simulations, starting in the S_1 state.

Following the ESPT in Time To monitor the progress of the ESPT, i.e., following the position of the transferred proton in time, different structural descriptors have been tested: (i) the O–H distance $d_{\mathrm{OH}}^{(\mathrm{X})} = |r_{\mathrm{H}} - r_{\mathrm{X}}|$ from the photoacid donor (X = D) or DMSO acceptor (X = A); (ii) a proton-transfer coordinate $\delta = (d_{\mathrm{OH}}^{(\mathrm{A})} - d_{\mathrm{OH}}^{(\mathrm{D})}) \cdot |r_{\mathrm{D}} - r_{\mathrm{A}}|^{-1}$ as frequently used in ground-state PT studies[69,70] and (iii) the O–H displacement $\Delta d_{\mathrm{OH}}^{(\mathrm{X})} = d_{\mathrm{OH}}^{(\mathrm{X})} - d_{\mathrm{OH}}^{(\mathrm{X})}(\mathrm{eq.})$ relative to its value at the optimized S_1(min) structure of **CPX**. The following discussion is mostly restricted to (ii), i.e., the PT coordinate, as this appears most useful to us. However, it is not as intuitive as the simple O–H distance (i). Still, alternative versions of all main plots using the other variables can be found in the SI.

The typical time evolution of the PT coordinate of a single trajectory is shown as the thin (red) line in Fig. 3(a). Two chemical states can be identified: The proton can either reside at the photoacid (state **I**: $\delta \sim -0.15$) or at the DMSO (state **II**: $\delta \sim +0.15$). A value of $\delta = 0$ would indicate that the proton is symmetrically shared between the donor and acceptor atoms. For both states (**I** and **II**), the values for the PT coordinate from a single trajectory seem to be, on average, slightly larger than the limiting values suggested by the optimized S_1 structures. A similar trend is observed in the O–H distance (cf. Fig. 3(b) and Fig. S2): The O–H distance matches well for the photoacid (ca. 1 Å), but is somewhat larger for DMSO (ca. 1.5 Å) in the non-transferred state (**II**). Another important feature of the behavior observed here is the highly dynamic character, i.e., the proton is constantly being transferred between the donor and acceptor in a single-trajectory picture.

Averaged over all trajectories, the evolution of the PT coordinate changes to a picture

https://doi.org/10.26434/chemrxiv-2025-90jkg **ORCID:** https://orcid.org/0000-0002-8734-5807 Content not peer-reviewed by ChemRxiv. **License:** CC BY 4.0

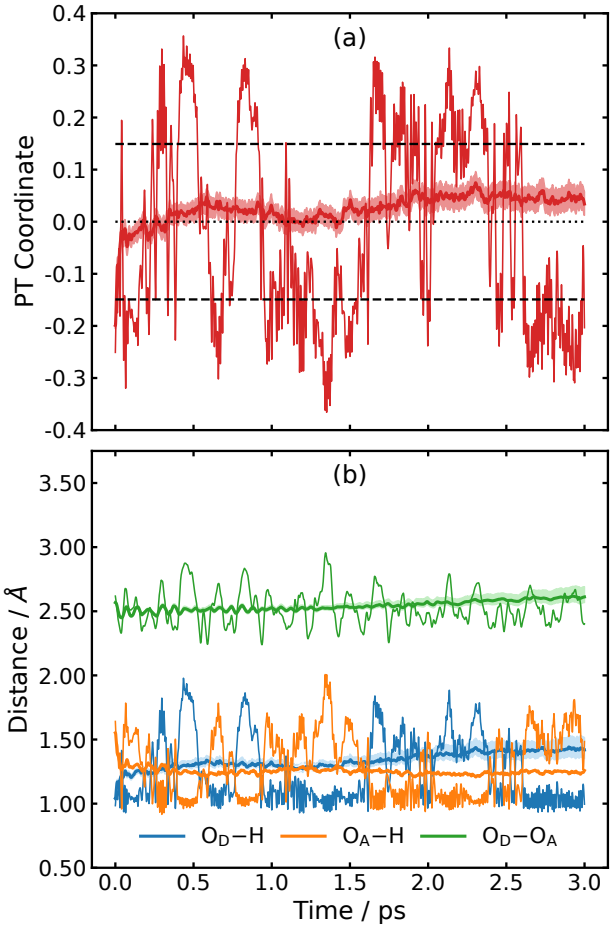


Figure 3: Time evolution of the proton-transfer (PT) coordinate δ (red), the O–H distances for the donor (blue) and acceptor (orange), and the donor-acceptor O–O distance (green) for a single trajectory (thin lines) and the ensemble average (thick lines) with the bootstrap confidence interval (95 %) as uncertainty estimate (areas). Black dashed lines (in a) indicate the minimum and maximum values from the optimized geometries (cf. Fig. 2) at ca. $\delta = \pm 0.15$ for reference.

represented by the thick (red) line in Fig. 3(a). Directly after excitation, the PT coordinate first undergoes an ultrafast (ca. 10 fs) increase from ca. -0.2 (i.e., smaller than at S_{min}) to ca. -0.1, mostly due to relaxation from the Franck-Condon point on the S_1 surface toward its minimum. Subsequently, the PT coordinate further increases, peaking at a positive value around 0.5 ps. Between 0.5 and 1.5 ps, the value decreases to zero before it continues to rise again, reaching a plateau after 3.0 ps. Although a value of $\delta \sim 0$ would indicate a symmetrically shared proton (i.e., a structure close to the transition state), the regions near

https://doi.org/10.26434/chemrxiv-2025-90jkg **ORCID:** https://orcid.org/0000-0002-8734-5807 Content not peer-reviewed by ChemRxiv. **License:** CC BY 4.0

zero should be better understood as the average between 50 % of trajectories that are in state **I** and 50 % that are in state **II**, giving rise to a zero mean value. Thus, the changes resulting from effective ESPT are, on average, rather subtle. We describe the changes shortly after excitation up to ca. 1.5 ps to the ESPT, converting the **CPX** into the **EC**, and those between 1.5 ps and 3.0 ps to a subsequent separation step, effectively further draining the **EC** population.

A comparative look at the O–H distances shows that the O–H acceptor distance is almost constant, whereas the donor distance continues to increase (cf. Fig. 3(b)). Moreover, a significant difference regarding the variability as quantified by the standard deviations (SDs) can be observed (cf. Fig. S2). While the SD of the O–H distance remains mostly constant for DMSO, it starts to significantly increase for the photoacid after 1.5 ps (Fig. S2(b)). This behavior could be traced back to some trajectories (see Fig. S3, SI) in which a roaming between the deprotonated photoacid and the protonated DMSO occurred after ESPT. However, the same trend persists even if these trajectories are excluded from the averaging (see Fig. S2(c), SI), showing that this behavior is only partially due to the roaming. We suspected an intermolecular translational-rotational motion as the origin of this behavior. To further investigate this, we calculated the distance and relative orientation between the photoacid and DMSO (excluding the transferred proton), defined in terms of the center-of-mass (COM) distances and an angle between the normal vector of the best-fitting ring plane and the direction vector of the S–O bond, respectively. As can be seen in Figs. S4 and S5 (SI), the distance between the centers changes only slowly (ca. 0.2 Å), while the relative orientation changes drastically ($> 10°$), especially after 1.5 ps. Altogether, these results indicate that the changes after 1.5 ps are predominantly due to an intramolecular rotation rather than a translation within the **EC**.

Besides, the O–H distance for DMSO shows an oscillation (up to 1 ps) with a period of ca. 60–70 fs, corresponding to 500–600 cm^{-1}, which is also visible in the donor–acceptor O–O distance (green plots in Fig. 3(b)). This frequency matches a ring skeletal mode (with

https://doi.org/10.26434/chemrxiv-2025-90jkg **ORCID:** https://orcid.org/0000-0002-8734-5807 Content not peer-reviewed by ChemRxiv. **License:** CC BY 4.0

the O_D and O_A approaching), which may assist the ESPT by lowering the effective energy barrier.

Correlating the Energy Gap with the Proton Distance Having demonstrated the usefulness of the PT coordinate for describing the different protonation states during the ESPT, we can now use it to replace the time coordinate, which leads to insightful correlations with the S_1–S_0 energy gap (see Fig. 4 and Fig. S6). This is particularly interesting as the S_1–S_0 energy gap depends on the current protonation state.

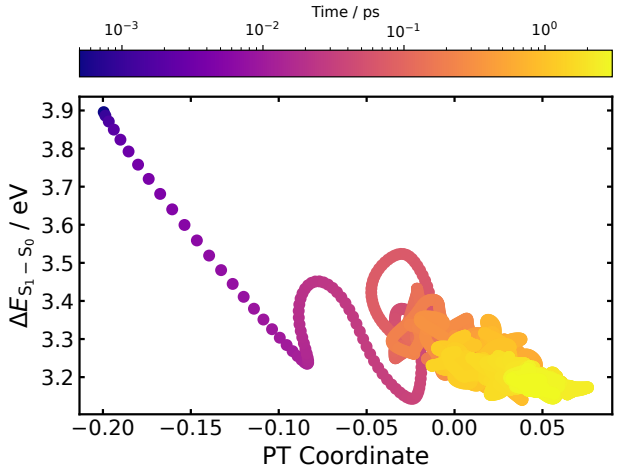


Figure 4: S_1–S_0 energy gap $\Delta E_{S_1-S_0}$ (in eV) as a function of the PT coordinate δ for the ensemble average. Time information is encoded by color, using a logarithmic scale, as indicated by the color bar.

Fig. 4 shows the mean S_1–S_0 energy gap plotted against the mean PT coordinate (averaged over all trajectories). A rapid decrease of the energy gap from ca. 3.9 eV (at $\delta = -0.2$) to ca. 3.2 eV (at $\delta = -0.1$) occurs within the first 20 fs. Then, the energy gap reveals an apparent barrier, increasing to a value of approximately 3.45 eV, while decreasing to a value of $\delta \sim -0.075$. Having passed the barrier, the energy gap drops to a value of < 3.2 eV (at $\delta = -0.025$) after 40 fs. From here on, the energy gap first increases to a value of ca. 3.5 eV, with the PT coordinate changing only slightly, and then becomes highly flexible. After these 100 fs, the energy gap decays from 3.4 eV (at $\delta = -0.025$) to an apparent asymptotic value of 3.15 eV at the largest value of the PT coordinate of ca. $\delta = -0.05$.

https://doi.org/10.26434/chemrxiv-2025-90jkg **ORCID:** https://orcid.org/0000-0002-8734-5807 Content not peer-reviewed by ChemRxiv. **License:** CC BY 4.0

The value of 3.9 eV is close to the emission energy at the Franck-Condon point directly after excitation (4.0 eV), whereas values of 3.5–3.6 eV and 3.2–3.3 eV are characteristic of **CPX** and **EC** near their S_1 minima, respectively. The simulation of the absorption and emission spectra from the initial conditions using the nuclear ensemble approach[71] reveals that the band maxima are approximately 0.1 eV lower than the vertical excitation energies (cf. Fig. S7, SI). In line with the previous discussion, we thus attribute the initial decay to the relaxation from the Franck-Condon point in combination with ultrafast ESPT within 50–100 fs, yielding the **EC**. Moreover, we ascribe the less pronounced changes between 0.1 ps and 1.0 ps to an equilibration between **CPX** and **EC**, explained as follows: Despite the effective barrier in $\Delta E_{S_1-S_0}$, a ballistic proton transfer takes place in most of the trajectories during the relaxation from FC due to the excessive kinetic energy, allowing it to almost instantaneously cross the barrier. As an endothermic process ($\Delta E = +3$ kJ mol^{-1}), the system can equilibrate from this non-equilibrium situation after the ESPT, converting some of the **EC** back into **CPX**. Additionally, **CPX** that has not initially reacted can perform an ESPT, yielding **EC** on the slower 0.1–1.0 ps timescale.

The even slower dynamics on the 1.0–3.0 ps timescale describe a subsequent effective separation of the **EC**. Interestingly, this clear initial progression is only observed in the ensemble average, but not in the individual trajectories, which is why we refer to it as a collective motion. The logarithmic color scale that decodes the time information (cf. Fig. 4) reveals a persistence of ca. 100 fs.

Excited-State Decay Kinetics For the closest possible comparison with the available experimental time-resolved fluorescence data by Kwon and coworkers,[42] we aimed to model the temporal decay of fluorescence intensity. In the first step, we calculated the populations of the different chemical species by applying energy windows (see Fig. 5). These allow for counting the populations based on the current value of the energy gap of each trajectory at a given time. To reduce the statistical noise, this counting is achieved in time bins of 10 fs,

https://doi.org/10.26434/chemrxiv-2025-90jkg **ORCID:** https://orcid.org/0000-0002-8734-5807 Content not peer-reviewed by ChemRxiv. **License:** CC BY 4.0

i.e., the check is performed in these bins and the counts are summed up. The corresponding populations of the different species are shown in Fig. 5(a–b).

The unrelaxed **CPX** (**CPX-FC**, in blue) is only present at time zero and disappears extremely fast, as expected. Surprisingly, the relaxed **CPX** (**CPX-Eq**, in orange) and the **EC** (in green) appear to have similar populations at the beginning. Whereas the population of **CPX(eq)** continuously decays to roughly half its initial value over the range of 3 ps, that of **EC** exhibits a weakly pronounced biphasic behavior with an initial rise within 1 ps and a subsequent slow decay. With the smallest energy gap, the population of a further separated species (**Sep**, in red) experiences a continuous increase over the full range of 3 ps, approaching ca. triple of its initial value of 2.5. As also demonstrated in Fig. 5(a), both the sum of the populations of all species as well as the partial sum of **CPX** and **EC** are reasonably constant, in line with proper counting. Interestingly, the initial decay of **CPX(FC)** does not yield a rise of **CPX(eq.)**, but rather **EC** and **Sep.**, pointing toward a direct ESPT during the relaxation.

Having the populations at hand, we calculated the fluorescence intensities. For this, we did not simply sum the counts in the time bins but instead weighted the counts by the spontaneous emission rate at the individual times (as opposed to weighting by 1, as for the populations).[72] The spontaneous emission rate for the $S_1 \rightarrow S_0$ transition is given by

$$\Gamma_{1\rightarrow 0} = \frac{2\alpha}{\hbar m_e c^2} \Delta E_{1\rightarrow 0}^2 f_{1\rightarrow 0}, \tag{2}$$

with $\Delta E_{1\rightarrow 0}$ and $f_{1\rightarrow 0}$ as, respectively, the energy and oscillator strength of the transition, and some natural constants (α: fine-structure constant; $\hbar$: reduced Planck constant; m_e: electron mass; c: speed of light). The corresponding time evolution of the simulated fluorescence intensity is shown in Fig. 5(c). Validation of the assignment of the chemical species based on the energy gap is further given by the correlation with the structural data (cf. Fig. S8, SI), revealing a nice clustering of the data points.

https://doi.org/10.26434/chemrxiv-2025-90jkg **ORCID:** https://orcid.org/0000-0002-8734-5807 Content not peer-reviewed by ChemRxiv. **License:** CC BY 4.0

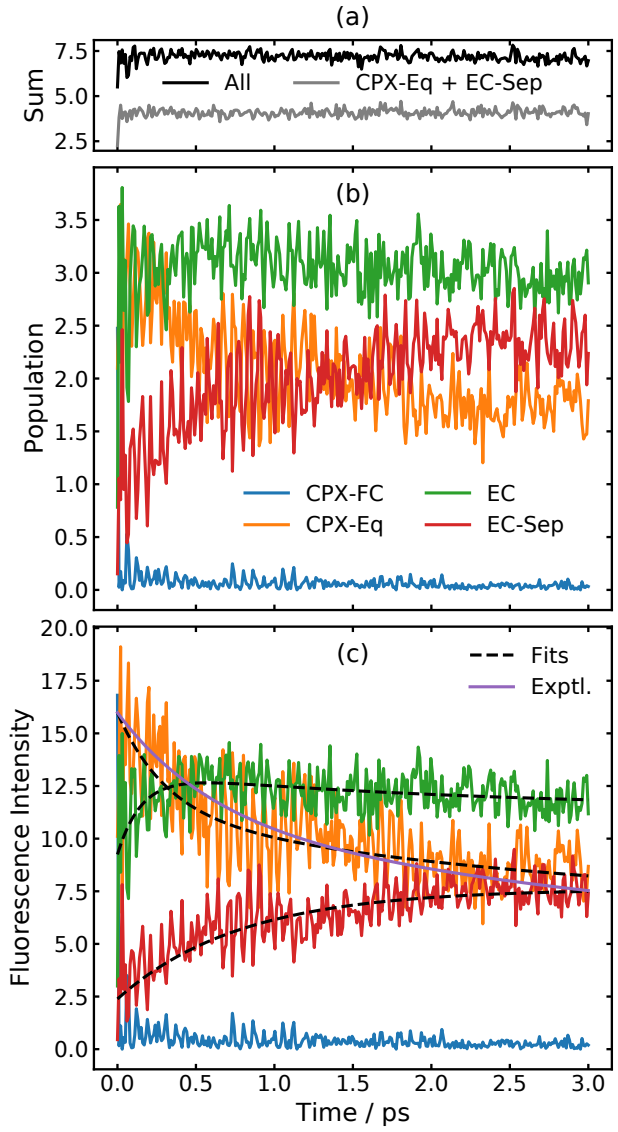


Figure 5: Time evolution of the sum (a) and individual populations (b), as well as the simulated fluorescence intensity (c) of the different chemical species defined based on energy windows. Each window is centered at a given value [CPX-Eq (3.90 eV), CPX-FC (3.47 eV), EC (3.20 eV), EC-Sep (3.00 eV)] and includes a width of ±0.05 eV. The tri-exponential decay reported by Kwon and co-workers is included as experimental reference.[42] Dashed lines indicate multi-exponential fits to the different decays (cf. Table 2).

https://doi.org/10.26434/chemrxiv-2025-90jkg **ORCID:** https://orcid.org/0000-0002-8734-5807 Content not peer-reviewed by ChemRxiv. **License:** CC BY 4.0

Qualitatively, the fluorescence intensity follows the same trends as the populations. The key message remains the same: **CPX** is effectively converting into **EC** and **Sep**. In analogy to what is done experimentally, we fitted the temporal fluorescence decays of **CPX(eq)**, **EC**, and **EC-Sep** to multi-exponential functions

$$I(t) = \sum_{i=0}^{N} A_i \exp(-t/\tau_i) = \sum_{i=0}^{N} A_i \exp(-k_i t) \tag{3}$$

with the amplitudes $\{A_i\}$ and lifetimes $\{\tau_i\}$ (or rate constants $\{k_i\}$) as parameters. The fits are determined by minimizing

$$\chi^2 = \sum_{j=1}^{n} \left(\frac{I_j^{(\mathrm{obs})} - I_j^{(\mathrm{fit})}}{\sigma_j} \right)^2 = \sum_{j=1}^{n} \left(\frac{r_j}{\sigma_j} \right)^2 \tag{4}$$

i.e., the sum of the residuals $r_j = I_j^{(\mathrm{obs})} - I_j^{(\mathrm{fit})}$ (as the differences between the observed and modeled fluorescence intensities) divided by the standard deviations of the error σ_j (taken from the ensemble averaging) for all n time bins. Due to its biphasic behavior, a bi-exponential fit ($N = 2$) is necessary for **EC**, while a mono-exponential fit ($N = 1$) is sufficient for **Sep**. In the case of **CPX(eq)**, both mono- and bi-exponential fits were performed. The optimized parameters are listed in Table 2.

Table 2: Results of the fits of the simulated fluorescence decay to multi-exponential functions (cf. Eq. (3)).

	A_0[a]	A_1	τ_1	A_2	τ_2	χ^2
CPX-Eq	8.412	6.564	711	—	—	2.120
CPX-Eq	6.649	4.597	305	4.734	2810	2.091
EC	12.247	−4.412	782	—	—	1.053
EC	11.414	−3.905	155	1.741	2146	1.036
EC-Sep	7.609	−5.222	782	—	—	2.232

[a] Constant offset (i.e., $\tau_0 \to \infty$)

CPX(eq) shows a slightly better agreement for a bi-exponential ($\chi^2 = 2.09$) than a mono-exponential ($\chi^2 = 2.12$) fit, revealing contributions with similar amplitudes from a faster (ca 0.3 ps) and a slower (ca 3 ps) contribution. In particular, the fast component

https://doi.org/10.26434/chemrxiv-2025-90jkg **ORCID:** https://orcid.org/0000-0002-8734-5807 Content not peer-reviewed by ChemRxiv. **License:** CC BY 4.0

is in fair agreement with the rise time (0.1–0.2 ps) of the **EC** signal from a bi-exponential fit. The **EC** decay is found to be ca 2 ps, which is comparable to that for the **CPX-Eq**. Restricting to the mono-exponential fits that capture the average lifetimes, the rise time of the **EC-Sep** signal (ca 1 ps) matches well the decay time of **CPX(eq)**, providing evidence for their mechanistic relation. However, the decay of **EC** does not match the rise of **EC-Sep**, as would be expected in the case of a sequential conversion, which may appear counterintuitive. We ascribe this paradox to a difference in the timescales and the establishment of chemical equilibrium in the excited state: After approximately 0.5 ps, the population and thus the signal of **EC** become constant, as an equilibrium between **CPX-Eq** and **EC** has been established due to the ESPT. Subsequently, i.e., from 1 ps on, the **EC** turns into **EC-Sep** due to the intramolecular rotation that separates the zwitterion of $NM7HQ^+$ from the protonated DMSO. Thus, effective conversion of **CPX-Eq** into **EC-Sep** is observed on the longer timescale—with the (mono-exponential) decay of **CPX-Eq** matching the rise of **EC-Sep**—and a roughly constant **EC** population.

Comparison with the previous experiments This interpretation is in agreement with the experimental results by Kwon and co-workers.[42] They reported a tri-exponential decay of the **CPX-Eq** signal (monitored at 450 nm) with fitted amplitudes 0.39, 0.48, and 0.36 and lifetimes 0.6 ps, 4 ps, and 110 ps, respectively. The first two were assigned to the ESPT of a *pre-equilibrium* (PE) between **CPX-Eq** and **EC**, while the slowest represents the **EC** decay. Their experimental fit (purple line in Fig. 5(c)) is in fair agreement with our bi-exponential fit to the simulated **CPX-Eq** decay. It should be noted that the slowest component (110 ps) is beyond the reach of our simulations, as it behaves quasi-constant up to the maximum simulation time of 3 ps. Moreover, Kwon and co-workers used the first two fast components to calculate an amplitude-weighted lifetime (AWL) according to

$$\tau_{\mathrm{ave}}^{(\mathrm{Kwon})} = \frac{A_1\tau_1 + A_2\tau_2}{A_1 + A_2} \tag{5}$$

https://doi.org/10.26434/chemrxiv-2025-90jkg **ORCID:** https://orcid.org/0000-0002-8734-5807 Content not peer-reviewed by ChemRxiv. **License:** CC BY 4.0

of 2.6 ps (i.e., 2–3 ps), describing the ESPT from the PE state. However, since their fit is tri-exponential, we rather suggest using a *fractional* AWL based on the full AWL

$$\tau_{\mathrm{ave}} = \frac{\sum_{i=1}^{N=3} A_i \tau_i}{\sum_{i=1}^{N=3} A_i} = \sum_{i=1}^{N=3} \frac{A_i}{\sum_{j=1}^{N=3} A_j} \tau_i = \sum_{i=1}^{N=3} f_i \tau_i \tag{6}$$

by truncating the summation at $N = 2$. Thereby, $\tau_{\mathrm{ave}}^{(1,2)} = f_1\tau_1 + f_2\tau_2 = 1.75$ ps includes all amplitudes in the denominator of the weighting factors f_i. The value of $\tau_{\mathrm{ave}}^{(1,2)}$ is slightly smaller than that of $\tau_{\mathrm{ave}}^{(\mathrm{Kwon})}$, in overall better agreement with our simulations (e.g., the mono-exponential fit). Still, we suggest not referring to these AWLs, but the pure lifetimes from the fits instead. As can be seen, both the fast (0.3 ps (sim.) vs. 0.6 ps (exptl.)) and the intermediate (2 ps (sim.) vs. 4 ps (exptl.)) components of the **CPX-Eq** decay are in good agreement between experiment and simulation.

While a timescale of 300 fs may appear relatively short for ESPT, approaching that of ESIPT (e.g., 50 fs for 3-hydroxyflavone),[64] similar ESPT lifetimes have been reported for other hydrogen-bonded systems. In general, such ultrafast ESPT requires either a particularly strong photoacid or Brønsted base. Very recently, Verma *et al.* reported ESPT of 4-hydroxychalcone ($\mathrm{p}K_{\mathrm{a}}^{*} \sim 0$) to 1-methyl-imidazole or tert-butyl amine within 500 fs,[73] which is comparable to that of $\mathrm{NM7HQ}^{+}$ ($\mathrm{p}K_{\mathrm{a}}^{*} \sim -2$) to DMSO studied here. Similarly, Grandjean *et al.* observed sub-ps ESPT for a hydroxypyrene-based super-photoacid ($\mathrm{p}K_{\mathrm{a}}^{*} \sim -3$) to trioctyl phosphine oxide (TOPO).[74] Similarly, Heo *et al.* found a coherent ESPT within 60 fs for the parent photoacid HPTS (8-hydroxypyrene-1,3,6-trisulfonate) ($\mathrm{p}K_{\mathrm{a}}^{*} \sim 1$) to acetate as a much stronger base.[61] Lastly, the ESPT of quinone cyanine 9 (QCy9), which is one of the strongest photoacids available ($\mathrm{p}K_{\mathrm{a}}^{*} \sim -8$), is known to take place within 50 fs in water.[75]

In summary, this work applies *ab initio* molecular dynamics (AIMD) using surface hopping to study the ultrafast dynamics of the excited-state proton transfer (ESPT) of the super-photoacid $\mathrm{NM7HQ}^{+}$ to the aprotic solvent DMSO. The simulations confirm a rapid equilibration between the photoacid–DMSO complex, **CPX**, and the so-called Eigen com-

https://doi.org/10.26434/chemrxiv-2025-90jkg **ORCID:** https://orcid.org/0000-0002-8734-5807 Content not peer-reviewed by ChemRxiv. **License:** CC BY 4.0

plex, **EC**, that is formed upon ESPT. Challenging previous assumptions, the ESPT is ultrafast (< 1 ps) and does not take place on a slower timescale of 2–3 ps, as deduced from experiments. Subsequently, the **EC** experiences a slow separation *via* a rotational motion (> 1 ps), even though no explicit solvent (i.e., directional specific interactions) is accounted for; as would be expected in reality. Interestingly, this finding bears a vague resemblance to the diffusive separation of the **EC** under the involvement of a second DMSO molecule into a Zundel-like cation, as observed in the experiments. Overall, this study provides additional information on the mechanistic details of the ESPT of super-photoacids in a non-aqueous solution.

As the main limitation of our approach, we identify the usage of a dielectric continuum solvent model. Due to their purely electrostatic nature, these models do not account for specific solvent–solute interactions, which are assumed to be most responsible for discrepancies compared to the experiment. Particularly, the encapsulation of the molecules within the solvent cavity causes an artificial binding that prevents complete separation (e.g., *via* diffusion). Thus, for future work, going beyond implicit solvation, e.g., by using mixed quantum-mechanical/molecular-mechanical (QM/MM) approaches, appears necessary for a better description of the local solvation (e.g., as done in Ref. 63). Such accurate, yet efficient approaches become even more important when studying larger systems like the related hydroxypyrene super-photoacids.[76–79]

Computational Methods

Static Calculations Before the AIMD simulations, we performed static quantum-chemical calculations to explore the reaction path for the ESPT reaction between $NM7HQ^+$ and DMSO. For this, we selected density functional theory (DFT) and time-dependent DFT (TDDFT)[80] with the long-range-separated, dispersion-corrected ωB97X-D functional[81,82] and the def2-SVP basis[83,84] set in combination with the conductor-like polarizable contin-

https://doi.org/10.26434/chemrxiv-2025-90jkg **ORCID:** https://orcid.org/0000-0002-8734-5807 Content not peer-reviewed by ChemRxiv. **License:** CC BY 4.0

uum model (C-PCM; in short: PCM)[85,86] for implicit solvation in DMSO ($\epsilon_r = 46.45$, $n = 1.479$)[66] as our target level of theory. The ORCA program (version 5.0.3)[87,88] was used due to the availability of PCM-TDDFT excited-state gradients,[89] employing the resolution-of-the-identity (RI) approximation (RIJONX)[90,91] and the Tamm-Dancoff approximation (TDA)[92] for TDDFT excitation energies. In addition, we exemplarily tested this level of theory against higher-level coupled-cluster methods and basis-set effects using TURBOMOLE (version 7.8).[93,94] For best comparison between ORCA and TURBOMOLE, the PCM parameters in ORCA were chosen to reproduce the results obtained with the related conductor-like screening model (COSMO)[95,96] in TURBOMOLE (see SI for further details).

UV/Vis absorption energies were calculated as (vertical) ($S_0 \rightarrow S_{n>0}$) excitation energies at equilibrium structures in the S_0 ground state (PCM non-equilibrium conditions), while fluorescence emission energies were calculated as ($S_1 \rightarrow S_0$) de-excitation energy at the S_1 equilibrium structure (PCM equilibrium conditions). S_1 structure optimizations invoked a total number of two excited states. The guess for the transition between the S_1 equilibrium structures before and after ESPT was taken from the minimum energy path obtained using the nudged elastic band climbing-image (NEB-CI) methods.

AIMD Simulations *Ab initio* non-adiabatic molecular dynamics simulations were performed using the Newton-X NS program (version 3.5.2)[97] with the fewest switches surface hopping (FSSH) algorithm,[51] combined with ORCA (version 6.0.1)[87,88] for the electronic structure. At the level mentioned above, i.e., PCM-RI-TDA-TDDFT(ωB97X-D)/def2-SVP, we simulated the dynamics in an implicit solution of 400 trajectories, each for 3 ps and with a 0.5 fs time step, starting in the S_1 state. The time-dependent Baeck-An (TDBA) approximation[98] was employed, approximating the nonadiabatic couplings as a function of the energy gaps and their second time derivatives. The use of surface hopping gives the system the possibility to switch into the S_0 ground state. However, no hops are observed in this study, and thus, the dynamics are effectively adiabatic. Initial conditions (1000) for the positions and

https://doi.org/10.26434/chemrxiv-2025-90jkg **ORCID:** https://orcid.org/0000-0002-8734-5807 Content not peer-reviewed by ChemRxiv. **License:** CC BY 4.0

velocities were generated from a quantum-harmonic oscillator Wigner distribution[71,99,100] based on the (harmonic) frequencies and normal modes of the NM7HQ$^+$–DMSO dimer at the S_0 equilibrium structure, using Nexton-X CS (version 2.6 (build 01, 2023-10-25)).[97,101] Hereby, both low- and high-frequency modes associated with the CH_3 in both NM7HQ$^+$ and DMSO were kept frozen, as suggested by Janoš *et al.*[102] Of these 1000 initial conditions, the 400 for trajectories were selected from the corresponding absorption spectrum with a center at 4.0 eV and an energy window of ±0.2 eV. Importantly, the parameter thresholds in ORCA for the DFT integration grids needed to be tightened to `defgrid-3` for a stable propagation with sufficient energy conservation.

Acknowledgement

N. S. thanks the Deutsche Forschungsgemeinschaft (DFG, German Research Foundation) for funding through project 388390466 (TRR 247). Computing resources have been provided by HPC@ZEMOS, through Germany's Excellence Strategy–EXC 2033–390677874–RESOLV. R. S. M. and M. B. received support from the French government under the France 2030 investment plan as part of the Initiative d'Excellence d'Aix-Marseille Université (A*MIDEX AMX-22-IN1-48). They acknowledge the Centre de Calcul Intensif d'Aix-Marseille for granting access to its high-performance computing resources.

Supporting Information Available

The following files are available free of charge.

- SI: (TDA-TDDFT) Determination of acidity jump ΔpK_a^* using the Förster cycle; (Different levels of theory) Benchmark calculations for the vertical excitation energies; [Additional Plots] Time evolution of O–H distance, PT coordinate, and O–H displacements (Ensemble average; EA); Time evolution of O–H displacement, ring–SO angle,

https://doi.org/10.26434/chemrxiv-2025-90jkg **ORCID:** https://orcid.org/0000-0002-8734-5807 Content not peer-reviewed by ChemRxiv. **License:** CC BY 4.0

and ring–SO distance (Individual trajectories; IT) ; Energy gap as a function of the O–H distance, PT coordinate, and O–H displacement (EA); UV/Vis absorption and fluorescence emission spectra simulated with nuclear ensemble approaches; Correlation of the simulated fluorescence intensity (EA); Time evolution of ring–SO angle, ring–SO distance (geometry center and center-of-mass), and ring atom RMSD (IT, EA). (PDF)

References

(1) Chou, P.-T.; Solntsev, K. M. Photoinduced Proton Transfer in Chemistry and Biology. *The Journal of Physical Chemistry B* **2015**, *119*, 2089–2089, Publisher: American Chemical Society.

(2) Kagel, H.; Frohme, M.; Glökler, J. Photoacids in biochemical applications. *Journal of Cellular Biotechnology* **2018**, *4*, 23–30, Publisher: IOS Press.

(3) Hammes-Schiffer, S. Virtual Issue on Proton Transfer. *The Journal of Physical Chemistry B* **2021**, *125*, 3725–3726, Publisher: American Chemical Society.

(4) Saway, J.; Salem, Z. M.; Badillo, J. J. Recent Advances in Photoacid Catalysis for Organic Synthesis. *Synthesis* **2021**, *53*, 489–497, Publisher: Georg Thieme Verlag KG.

(5) Shabani, M.; Younesi, H.; Pontié, M.; Rahimpour, A.; Rahimnejad, M.; Zinatizadeh, A. A. A critical review on recent proton exchange membranes applied in microbial fuel cells for renewable energy recovery. *Journal of Cleaner Production* **2020**, *264*, 121446.

(6) Neupane, P.; Bhuju, S.; Thapa, N.; Bhattarai, H. K. ATP Synthase: Structure, Function and Inhibition. *Biomolecular Concepts* **2019**, *10*, 1–10, Publisher: De Gruyter.

https://doi.org/10.26434/chemrxiv-2025-90jkg **ORCID:** https://orcid.org/0000-0002-8734-5807 Content not peer-reviewed by ChemRxiv. **License:** CC BY 4.0

(7) Ghosh, I.; Khan, S.; Banerjee, G.; Dziarski, A.; Vinyard, D. J.; Debus, R. J.; Brudvig, G. W. Insights into Proton-Transfer Pathways during Water Oxidation in Photosystem II. *The Journal of Physical Chemistry B* **2019**, *123*, 8195–8202, Publisher: American Chemical Society.

(8) Laptenok, S. P.; Conyard, J.; Bulman Page, P. C.; Chan, Y.; You, M.; R. Jaffrey, S.; R. Meech, S. Photoacid behaviour in a fluorinated green fluorescent protein chromophore: ultrafast formation of anion and zwitterion states. *Chemical Science* **2016**, *7*, 5747–5752, Publisher: Royal Society of Chemistry.

(9) Chen, C.; Zhu, L.; Baranov, M. S.; Tang, L.; Baleeva, N. S.; Smirnov, A. Y.; Yampolsky, I. V.; Solntsev, K. M.; Fang, C. Photoinduced Proton Transfer of GFP-Inspired Fluorescent Superphotoacids: Principles and Design. *The Journal of Physical Chemistry B* **2019**, *123*, 3804–3821, Publisher: American Chemical Society.

(10) Snellenburg, J. J.; Laptenok, S. P.; DeSa, R. J.; Naumov, P.; Solntsev, K. M. Excited-State Dynamics of Oxyluciferin in Firefly Luciferase. *Journal of the American Chemical Society* **2016**, *138*, 16252–16258, Publisher: American Chemical Society.

(11) Yucknovsky, A.; Amdursky, N. Photoacids and Photobases: Applications in Functional Dynamic Systems. *Angewandte Chemie* **2025**, *137*, e202422963.

(12) Sülzner, N.; Jung, G.; Nuernberger, P. A dual experimental–theoretical perspective on ESPT photoacids and their challenges ahead. *Chemical Science* **2025**, *16*, 1560–1596.

(13) Saway, J.; F. Pierre, A.; J. Badillo, J. Photoacid-catalyzed acetalization of carbonyls with alcohols. *Organic & Biomolecular Chemistry* **2022**, *20*, 6188–6192, Publisher: Royal Society of Chemistry.

(14) Finkler, B.; Riemann, I.; Vester, M.; Grüter, A.; Stracke, F.; Jung, G. Monomolecular pyrenol-derivatives as multi-emissive probes for orthogonal reactivities. *Photochemical & Photobiological Sciences* **2016**, *15*, 1544–1557.

https://doi.org/10.26434/chemrxiv-2025-90jkg **ORCID:** https://orcid.org/0000-0002-8734-5807 Content not peer-reviewed by ChemRxiv. **License:** CC BY 4.0

(15) Menges, J. A.; Clasen, A.; Jourdain, M.; Beckmann, J.; Hoffmann, C.; König, J.; Jung, G. Surface Preparation for Single-Molecule Chemistry. *Langmuir* **2019**, *35*, 2506–2516, Publisher: American Chemical Society.

(16) Eigen, M.; Kruse, W.; Maass, G.; Demaeyer, L. Rate Constants of Protolytic Reactions in Aqueous Solution. *Progress in Reaction Kinetics and Mechanism* **1964**, *2*, 285–&, Place: Northwood Publisher: Science & Technology Letters WOS:A1964WS99500006.

(17) Weller, A. Fast Reactions of Excited Molecules. *Progress in Reaction Kinetics and Mechanism* **1961**, *1*, 187–&, Place: Northwood Publisher: Science & Technology Letters WOS:A1961WS99400007.

(18) Leiderman, P.; Genosar, L.; Huppert, D. Excited-State Proton Transfer: Indication of Three Steps in the Dissociation and Recombination Process. *The Journal of Physical Chemistry A* **2005**, *109*, 5965–5977, Publisher: American Chemical Society.

(19) Tolbert, L. M.; Solntsev, K. M. Excited-State Proton Transfer: From Constrained Systems to "Super" Photoacids to Superfast Proton Transfer. *Accounts of Chemical Research* **2002**, *35*, 19–27.

(20) Park, S.-Y.; Lee, Y. M.; Kwac, K.; Jung, Y.; Kwon, O.-H. Alcohol Dimer is Requisite to Form an Alkyl Oxonium Ion in the Proton Transfer of a Strong (Photo)Acid to Alcohol. *Chemistry – A European Journal* **2016**, *22*, 4340–4344.

(21) Kim, T. G.; Topp, M. R. Ultrafast Excited-State Deprotonation and Electron Transfer in Hydroxyquinoline Derivatives. *The Journal of Physical Chemistry A* **2004**, *108*, 10060–10065.

(22) Bardez, E.; Devol, I.; Larrey, B.; Valeur, B. Excited-State Processes in 8-Hydroxyquinoline: Photoinduced Tautomerization and Solvation Effects. *The Journal of Physical Chemistry B* **1997**, *101*, 7786–7793, Publisher: American Chemical Society.

https://doi.org/10.26434/chemrxiv-2025-90jkg **ORCID:** https://orcid.org/0000-0002-8734-5807 Content not peer-reviewed by ChemRxiv. **License:** CC BY 4.0

(23) Codescu, M.-A.; Weiß, M.; Brehm, M.; Kornilov, O.; Sebastiani, D.; Nibbering, E. T. J. Switching between Proton Vacancy and Excess Proton Transfer Pathways in the Reaction between 7-Hydroxyquinoline and Formate. *The Journal of Physical Chemistry A* **2021**, *125*, 1845–1859, Publisher: American Chemical Society.

(24) Franz, J.; Peyerimhoff, S. D.; Hanrath, M.; Kwon, O.-H.; Jang, D.-J. Ab Initio Study of the Electronic Spectrum of 7-Hydroxyquinoline. *Chemistry Letters* **2005**, *34*, 330–331, Publisher: The Chemical Society of Japan.

(25) Park, H. J.; Kwon, O.-H.; Ah, C. S.; Jang, D.-J. Excited-State Tautomerization Dynamics of 7-Hydroxyquinoline in β-Cyclodextrin. *The Journal of Physical Chemistry B* **2005**, *109*, 3938–3943, Publisher: American Chemical Society.

(26) Kwon, O.-H.; Kim, T. G.; Lee, Y.-S.; Jang, D.-J. Biphasic Tautomerization Dynamics of Excited 7-Hydroxyquinoline in Reverse Micelles. *The Journal of Physical Chemistry B* **2006**, *110*, 11997–12004, Publisher: American Chemical Society.

(27) Kwon, O.-H.; Lee, Y.-S.; Yoo, B. K.; Jang, D.-J. Excited-State Triple Proton Transfer of 7-Hydroxyquinoline along a Hydrogen-Bonded Alcohol Chain: Vibrationally Assisted Proton Tunneling. *Angewandte Chemie* **2006**, *118*, 429–433, _eprint: https://onlinelibrary.wiley.com/doi/pdf/10.1002/ange.200503209.

(28) Park, K.; Shin, K. J.; Kim, H. Excited-state reversible geminate recombination in two dimensions. *The Journal of Chemical Physics* **2009**, *131*, 154105.

(29) Park, S.-Y.; Kwon, O.-H.; Kim, T. G.; Jang, D.-J. Ground-State Proton Transfer of 7-Hydroxyquinoline Confined in Biologically Relevant Water Nanopools. *The Journal of Physical Chemistry C* **2009**, *113*, 16110–16115, Publisher: American Chemical Society.

(30) Park, S.-Y.; Lee, Y.-S.; Kwon, O.-H.; Jang, D.-J. Proton transport of water in acid–

https://doi.org/10.26434/chemrxiv-2025-90jkg **ORCID:** https://orcid.org/0000-0002-8734-5807 Content not peer-reviewed by ChemRxiv. **License:** CC BY 4.0

base reactions of 7-hydroxyquinoline. *Chemical Communications* **2009**, *0*, 926–928, Publisher: Royal Society of Chemistry.

(31) Park, S.-Y.; Kim, B.; Lee, Y.-S.; Kwon, O.-H.; Jang, D.-J. Triple proton transfer of excited 7-hydroxyquinoline along a hydrogen -bonded water chain in ethers: secondary solvent effect on the reaction rate. *Photochemical & Photobiological Sciences* **2009**, *8*, 1611–1617.

(32) Kim, Y.-J.; Kwon, O.-H. Proton diffusion dynamics along a diol as a proton-conducting wire in a photo-amphiprotic model system. *Physical Chemistry Chemical Physics* **2016**, *18*, 32826–32839, Publisher: The Royal Society of Chemistry.

(33) Park, S.-Y.; Kwon, O.-H.; Lee, Y.-S.; Jang, D.-J. Triplet-State Acid–Base Reactions of 1-Methyl-7-oxyquinolinium in Water. *The Journal of Physical Chemistry A* **2009**, *113*, 10589–10592, Publisher: American Chemical Society.

(34) Lee, Y. M.; Park, S.-Y.; Kim, H.; Kim, T. G.; Kwon, O.-H. Photoinduced strong acid–weak base reactions in a polar aprotic solvent. *Methods and Applications in Fluorescence* **2016**, *4*, 024004.

(35) Park, S.-Y.; Kim, T. G.; Ajitha, M. J.; Kwac, K.; Lee, Y. M.; Kim, H.; Jung, Y.; Kwon, O.-H. The critical size of hydrogen-bonded alcohol clusters as effective Brønsted bases in solutions. *Physical Chemistry Chemical Physics* **2016**, *18*, 24880–24889.

(36) Kim, Y.-J.; Rakshit, S.; Jin, G. Y.; Ghosh, P.; Lee, Y. M.; Park, W.-W.; Kim, Y. S.; Kwon, O.-H. Synergistic Configuration of Diols as Brønsted Bases. *Chemistry – A European Journal* **2017**, *23*, 17179–17185, _eprint: https://onlinelibrary.wiley.com/doi/pdf/10.1002/chem.201703668.

(37) Adhikari, A.; Park, J.-H.; Nho, H.-W.; Kwon, O.-H. Residence and diffusion of a dynamically prototropic hydration probe in AOT reverse micelles. *Journal of Molecular Liquids* **2020**, *320*, 114346.

https://doi.org/10.26434/chemrxiv-2025-90jkg **ORCID:** https://orcid.org/0000-0002-8734-5807 Content not peer-reviewed by ChemRxiv. **License:** CC BY 4.0

(38) Nho, H.-W.; Park, J.-H.; Adhikari, A.; Kwon, O.-H. Acid–base reaction of a cationic hydration probe in vicinity of anionic interface of AOT reverse micelles. *Journal of Molecular Liquids* **2021**, *326*, 115270.

(39) Nho, H.-W.; Adhikari, A.; Kwon, O.-H. Ultrafast Excited-State Proton Transfer of a Cationic Superphotoacid in a Nanoscopic Water Pool. *The Journal of Physical Chemistry B* **2022**, *126*, 1275–1283.

(40) Choi, Y.; Kim, H.; Kwon, O. Acid–base reaction of a super-photoacid with a cooperative amide hydrogen-bonded chain. *Bulletin of the Korean Chemical Society* **2022**, *43*, 501–507.

(41) Choi, Y.-J.; Nho, H.-W.; Kim, Y.-J.; Kwon, O.-H. Quantifying the Ground-State Hydrogen-Bond Formation of a Super-Photoacid by Inspecting Its Excited-State Dynamics. *ChemPhotoChem* **2024**, *8*, e202300164, _eprint: https://onlinelibrary.wiley.com/doi/pdf/10.1002/cptc.202300164.

(42) Lee, S.-H.; Choi, Y.-J.; Kim, Y.-J.; Kee, J.-M.; Kwon, O.-H. Capturing an Eigen complex in an acid-base reaction shows step-resolved molecularity. *Cell Reports Physical Science* **2024**, *5*, 102155.

(43) Lee, S.-W.; Kwon, O.-H. Lifetimes and Lifetime-Associated Spectra for Reversible Excited Two-State Reactions. *The Journal of Physical Chemistry A* **2025**, *129*, 447–458.

(44) Note that NM7HQ$^+$ is not referred to as a *cationic* photoacid since this term is used in the literature only for photoacids with a positively charged acidic group (e.g., NH_3^+), independent of the total charge.

(45) Sülzner, N. New light on proton transfer: Spectral and kinetic signature of a transient Eigen complex. *Chem* **2024**, *10*, 3276–3278.

https://doi.org/10.26434/chemrxiv-2025-90jkg **ORCID:** https://orcid.org/0000-0002-8734-5807 Content not peer-reviewed by ChemRxiv. **License:** CC BY 4.0

(46) Simkovitch, R.; Shomer, S.; Gepshtein, R.; Huppert, D. How Fast Can a Proton-Transfer Reaction Be beyond the Solvent-Control Limit? *The Journal of Physical Chemistry B* **2015**, *119*, 2253–2262.

(47) Xia, S.-H.; Xie, B.-B.; Fang, Q.; Cui, G.; Thiel, W. Excited-state intramolecular proton transfer to carbon atoms: nonadiabatic surface-hopping dynamics simulations. *Physical Chemistry Chemical Physics* **2015**, *17*, 9687–9697, Publisher: Royal Society of Chemistry.

(48) Guo, W.-W.; Liu, X.-Y.; Chen, W.-K.; Cui, G. Excited-state proton transfer in 4-2'-hydroxyphneylpyridine: full-dimensional surface-hopping dynamics simulations. *RSC Advances* **2016**, *6*, 85574–85581, Publisher: Royal Society of Chemistry.

(49) Jankowska, J.; Barbatti, M.; Sadlej, J.; Sobolewski, A. L. Tailoring the Schiff base photoswitching – a non-adiabatic molecular dynamics study of substituent effect on excited state proton transfer. *Physical Chemistry Chemical Physics* **2017**, *19*, 5318–5325, Publisher: The Royal Society of Chemistry.

(50) Crespo-Otero, R.; Barbatti, M. Recent Advances and Perspectives on Nonadiabatic Mixed Quantum–Classical Dynamics. *Chemical Reviews* **2018**, *118*, 7026–7068.

(51) Tully, J. C. Molecular dynamics with electronic transitions. *The Journal of Chemical Physics* **1990**, *93*, 1061–1071.

(52) M. Toldo, J.; Casal, M. T. d.; Ventura, E.; Monte, S. A. d.; Barbatti, M. Surface hopping modeling of charge and energy transfer in active environments. *Physical Chemistry Chemical Physics* **2023**, *25*, 8293–8316.

(53) Guglielmi, M.; Tavernelli, I.; Rothlisberger, U. On the proton transfer mechanism in ammonia-bridged 7-hydroxyquinoline: a TDDFT molecular dynamics study. *Physical Chemistry Chemical Physics* **2009**, *11*, 4549–4555, Publisher: The Royal Society of Chemistry.

https://doi.org/10.26434/chemrxiv-2025-90jkg **ORCID:** https://orcid.org/0000-0002-8734-5807 Content not peer-reviewed by ChemRxiv. **License:** CC BY 4.0

(54) Bekçioğlu, G.; Hoffmann, F.; Sebastiani, D. Solvation-Dependent Latency of Photoacid Dissociation and Transient IR Signatures of Protonation Dynamics. *The Journal of Physical Chemistry A* **2015**, *119*, 9244–9251, Publisher: American Chemical Society.

(55) Petrone, A.; Donati, G.; Caruso, P.; Rega, N. Understanding THz and IR Signals beneath Time-Resolved Fluorescence from Excited-State Ab Initio Dynamics. *Journal of the American Chemical Society* **2014**, *136*, 14866–14874, Publisher: American Chemical Society.

(56) Chiariello, M. G.; Rega, N. Exploring Nuclear Photorelaxation of Pyranine in Aqueous Solution: an Integrated Ab-Initio Molecular Dynamics and Time Resolved Vibrational Analysis Approach. *The Journal of Physical Chemistry A* **2018**, *122*, 2884–2893.

(57) Chiariello, M. G.; Donati, G.; Raucci, U.; Perrella, F.; Rega, N. Structural Origin and Vibrational Fingerprints of the Ultrafast Excited State Proton Transfer of the Pyranine-Acetate Complex in Aqueous Solution. *The Journal of Physical Chemistry B* **2021**, *125*, 10273–10281.

(58) Chiariello, M. G.; Donati, G.; Rega, N. Time-Resolved Vibrational Analysis of Excited State Ab Initio Molecular Dynamics to Understand Photorelaxation: The Case of the Pyranine Photoacid in Aqueous Solution. *Journal of Chemical Theory and Computation* **2020**, *16*, 6007–6013.

(59) Chiariello, M. G.; Raucci, U.; Donati, G.; Rega, N. Water-Mediated Excited State Proton Transfer of Pyranine–Acetate in Aqueous Solution: Vibrational Fingerprints from Ab Initio Molecular Dynamics. *The Journal of Physical Chemistry A* **2021**, *125*, 3569–3578.

(60) Raucci, U.; Chiariello, M. G.; Rega, N. Modeling Excited-State Proton Transfer to

https://doi.org/10.26434/chemrxiv-2025-90jkg **ORCID:** https://orcid.org/0000-0002-8734-5807 Content not peer-reviewed by ChemRxiv. **License:** CC BY 4.0

Solvent: A Dynamics Study of a Super Photoacid with a Hybrid Implicit/Explicit Solvent Model. *Journal of Chemical Theory and Computation* **2020**, *16*, 7033–7043.

(61) Heo, W.; Uddin, N.; Park, J. W.; Rhee, Y. M.; Choi, C. H.; Joo, T. Coherent intermolecular proton transfer in the acid–base reaction of excited state pyranine. *Physical Chemistry Chemical Physics* **2017**, *19*, 18243–18251.

(62) Thomaz, J. E.; Walker, A. R.; Van Wyck, S. J.; Meisner, J.; Martinez, T. J.; Fayer, M. D. Proton Transfer Dynamics in the Aprotic Proton Accepting Solvent 1-Methylimidazole. *The Journal of Physical Chemistry B* **2020**, *124*, 7897–7908.

(63) Walker, A. R.; Wu, B.; Meisner, J.; Fayer, M. D.; Martínez, T. J. Proton Transfer from a Photoacid to a Water Wire: First Principles Simulations and Fast Fluorescence Spectroscopy. *The Journal of Physical Chemistry B* **2021**, *125*, 12539–12551.

(64) Li, Y.; Siddique, F.; Aquino, A. J. A.; Lischka, H. Molecular Dynamics Simulation of the Excited-State Proton Transfer Mechanism in 3-Hydroxyflavone Using Explicit Hydration Models. *The Journal of Physical Chemistry A* **2021**, *125*, 5765–5778, Publisher: American Chemical Society.

(65) Olmsted, J. Effect of refractive index on molecular radiative lifetimes. *Chemical Physics Letters* **1976**, *38*, 287–292.

(66) Spies, C.; Finkler, B.; Acar, N.; Jung, G. Solvatochromism of pyranine-derived photoacids. *Physical Chemistry Chemical Physics* **2013**, *15*, 19893.

(67) Pines, D.; Pines, E. *Hydrogen-Transfer Reactions*; John Wiley & Sons, Ltd, 2006; pp 377–415, Section: 12 _eprint: https://onlinelibrary.wiley.com/doi/pdf/10.1002/9783527611546.ch12.

(68) Karbalaei Khani, S.; Marefat Khah, A.; Hättig, C. Comparison of Reaction Field Schemes for Coupling Continuum Solvation Models with Wave Function Methods for

https://doi.org/10.26434/chemrxiv-2025-90jkg **ORCID:** https://orcid.org/0000-0002-8734-5807 Content not peer-reviewed by ChemRxiv. **License:** CC BY 4.0

Excitation Energies. *Journal of Chemical Theory and Computation* **2020**, *16*, 4554–4564.

(69) Marx, D. Proton Transfer 200 Years after von Grotthuss: Insights from Ab Initio Simulations. *ChemPhysChem* **2006**, *7*, 1848–1870.

(70) Marx, D. Proton Transfer 200 Years after von Grotthuss: Insights from Ab Initio Simulations. *ChemPhysChem* **2007**, *8*, 209–210.

(71) Crespo-Otero, R.; Barbatti, M. Spectrum simulation and decomposition with nuclear ensemble: formal derivation and application to benzene, furan and 2-phenylfuran. *Theoretical Chemistry Accounts* **2012**, *131*, 1237.

(72) Braun, G.; Borges, J., Itamar; Aquino, A. J. A.; Lischka, H.; Plasser, F.; do Monte, S. A.; Ventura, E.; Mukherjee, S.; Barbatti, M. Non-Kasha fluorescence of pyrene emerges from a dynamic equilibrium between excited states. *The Journal of Chemical Physics* **2022**, *157*, 154305.

(73) Verma, P.; Mathew, R.; Dhiman, N.; Mitra, P. K.; Lakshmanna, Y. A. Ultrafast excited-state dynamics of 4-hydroxychalcone: role of intramolecular charge transfer and photoacidity. *Physical Chemistry Chemical Physics* **2025**, *27*, 7716–7727.

(74) Grandjean, A.; Pérez Lustres, J. L.; Jung, G. Solvent-Controlled Intermolecular Proton-Transfer Follows an Irreversible Eigen-Weller Model from fs to ns. *ChemPhotoChem* **2021**, *5*, 1094–1105.

(75) Simkovitch, R.; Shomer, S.; Gepshtein, R.; Shabat, D.; Huppert, D. Excited-State Proton Transfer from Quinone-Cyanine 9 to Protic Polar-Solvent Mixtures. *The Journal of Physical Chemistry A* **2014**, *118*, 1832–1840.

(76) Sülzner, N.; Geissler, B.; Grandjean, A.; Jung, G.; Nuernberger, P. Excited-State Proton Transfer Dynamics of a Super-Photoacid in Acetone-

https://doi.org/10.26434/chemrxiv-2025-90jkg **ORCID:** https://orcid.org/0000-0002-8734-5807 Content not peer-reviewed by ChemRxiv. **License:** CC BY 4.0

Water Mixtures. *ChemPhotoChem* **2022**, *6*, e202200041, _eprint: https://onlinelibrary.wiley.com/doi/pdf/10.1002/cptc.202200041.

(77) Knorr, J.; Sülzner, N.; Geissler, B.; Spies, C.; Grandjean, A.; Kutta, R. J.; Jung, G.; Nuernberger, P. Ultrafast transient absorption and solvation of a super-photoacid in acetoneous environments. *Photochemical & Photobiological Sciences* **2022**, *21*, 2179–2192.

(78) Sülzner, N.; Hättig, C. Theoretical Study on the Photoacidity of Hydroxypyrene Derivatives in DMSO Using ADC(2) and CC2. *The Journal of Physical Chemistry A* **2022**, *126*, 5911–5923, Publisher: American Chemical Society.

(79) Sülzner, N.; Hättig, C. Computational investigation of explicit solvent effects and specific interactions of hydroxypyrene photoacids in acetone, DMSO, and water. *Physical Chemistry Chemical Physics* **2023**, *25*, 11130–11144, Publisher: The Royal Society of Chemistry.

(80) Petrenko, T.; Kossmann, S.; Neese, F. Efficient time-dependent density functional theory approximations for hybrid density functionals: Analytical gradients and parallelization. *J. Chem. Phys.* **2011**, *134*, 054116.

(81) Chai, J.-D.; Head-Gordon, M. Long-range corrected hybrid density functionals with damped atom–atom dispersion corrections. *Physical Chemistry Chemical Physics* **2008**, *10*, 6615–6620.

(82) Grimme, S.; Antony, J.; Ehrlich, S.; Krieg, H. A consistent and accurate ab initio parametrization of density functional dispersion correction (DFT-D) for the 94 elements H-Pu. *The Journal of Chemical Physics* **2010**, *132*, 154104.

(83) Weigend, F.; Ahlrichs, R. Balanced basis sets of split valence, triple zeta valence and quadruple zeta valence quality for H to Rn: Design and assessment of accuracy. *Physical Chemistry Chemical Physics* **2005**, *7*, 3297–3305.

https://doi.org/10.26434/chemrxiv-2025-90jkg **ORCID:** https://orcid.org/0000-0002-8734-5807 Content not peer-reviewed by ChemRxiv. **License:** CC BY 4.0

(84) Weigend, F. Accurate Coulomb-fitting basis sets for H to Rn. *Physical Chemistry Chemical Physics* **2006**, *8*, 1057–1065.

(85) Cossi, M.; Rega, N.; Scalmani, G.; Barone, V. Energies, structures, and electronic properties of molecules in solution with the C-PCM solvation model. *Journal of Computational Chemistry* **2003**, *24*, 669–681.

(86) Mennucci, B. Polarizable continuum model. *WIREs Computational Molecular Science* **2012**, *2*, 386–404.

(87) Neese, F. The ORCA program system. *WIRES Comput. Molec. Sci.* **2012**, *2*, 73–78.

(88) Neese, F. Software update: the ORCA program system, version 5.0. *WIRES Comput. Molec. Sci.* **2022**, *12*, e1606.

(89) Garcia-Rates, M.; Neese, F. Effect of the Solute Cavity on the Solvation Energy and its Derivatives within the Framework of the Gaussian Charge Scheme. *J. Comput. Chem.* **2020**, *41*, 922–939.

(90) Neese, F. An improvement of the resolution of the identity approximation for the formation of the Coulomb matrix. *J. Comp. Chem.* **2003**, *24*, 1740–1747.

(91) Neese, F.; Olbrich, G. Efficient use of the resolution of the identity approximation in time-dependent density functional calculations with hybrid density functionals. *Chem. Phys. Lett.* **2002**, *362*, 170–178.

(92) Hirata, S.; Head-Gordon, M. Time-dependent density functional theory within the Tamm–Dancoff approximation. *Chemical Physics Letters* **1999**, *314*, 291–299.

(93) TURBOMOLE V7.7 2023, a development of University of Karlsruhe and Forschungszentrum Karlsruhe GmbH, 1989-2007, TURBOMOLE GmbH, since 2007; available from

`https://www.turbomole.org`.

https://doi.org/10.26434/chemrxiv-2025-90jkg **ORCID:** https://orcid.org/0000-0002-8734-5807 Content not peer-reviewed by ChemRxiv. **License:** CC BY 4.0

(94) Franzke, Y. J.; Holzer, C.; Andersen, J. H.; Begušić, T.; Bruder, F.; Coriani, S.; Della Sala, F.; Fabiano, E.; Fedotov, D. A.; Fürst, S. et al. TURBOMOLE: Today and Tomorrow. *Journal of Chemical Theory and Computation* **2023**, *19*, 6859–6890.

(95) Schäfer, A.; Klamt, A.; Sattel, D.; Lohrenz, J. C. W.; Eckert, F. COSMO Implementation in TURBOMOLE: Extension of an efficient quantum chemical code towards liquid systems. *Physical Chemistry Chemical Physics* **2000**, *2*, 2187–2193, Publisher: The Royal Society of Chemistry.

(96) Klamt, A. The COSMO and COSMO-RS solvation models. *WIREs Computational Molecular Science* **2018**, *8*, e1338.

(97) Barbatti, M.; Bondanza, M.; Crespo-Otero, R.; Demoulin, B.; Dral, P. O.; Granucci, G.; Kossoski, F.; Lischka, H.; Mennucci, B.; Mukherjee, S. et al. Newton-X Platform: New Software Developments for Surface Hopping and Nuclear Ensembles. *Journal of Chemical Theory and Computation* **2022**, *18*, 6851–6865.

(98) T. do Casal, M.; Toldo, J.; Pinheiro Jr, M.; Barbatti, M. Fewest switches surface hopping with Baeck-An couplings [version 2; peer review: 3 approved]. *Open Research Europe* **2022**, *1*.

(99) Hillery, M.; O'Connell, R. F.; Scully, M. O.; Wigner, E. P. Distribution functions in physics: Fundamentals. *Physics Reports* **1984**, *106*, 121–167.

(100) Case, W. B. Wigner functions and Weyl transforms for pedestrians. *American Journal of Physics* **2008**, *76*, 937–946.

(101) Barbatti, M.; Granucci, G.; Ruckenbauer, M.; Plasser, R., F.and Crespo-Otero; Pittner, J.; Persico, M.; Lischka, H. NEWTON-X: A package for Newtonian dynamics close to the crossing seam. Version 2, 2016, www.newtonx.org.

https://doi.org/10.26434/chemrxiv-2025-90jkg **ORCID:** https://orcid.org/0000-0002-8734-5807 Content not peer-reviewed by ChemRxiv. **License:** CC BY 4.0

(102) Janoš, J.; Slavíček, P.; Curchod, B. F. E. Selecting Initial Conditions for Trajectory-Based Nonadiabatic Simulations. *Accounts of Chemical Research* **2025**, *58*, 261–270.

https://doi.org/10.26434/chemrxiv-2025-90jkg **ORCID:** https://orcid.org/0000-0002-8734-5807 Content not peer-reviewed by ChemRxiv. **License:** CC BY 4.0